Improvement of microstructure of amorphous silicon–germanium alloys by hydrogen dilution

A. R. Middya and Swati Ray
Energy Research Unit, Indian Association for the Cultivation of Science, Jadavpur, Calcutta 700 032, India

S. J. Jones[a] and D. L. Williamson[b]
Department of Physics, Colorado School of Mines, Golden, Colorado 80401

(Received 24 March 1995; accepted for publication 30 June 1995)

The microstructures of two sets of hydrogenated amorphous silicon–germanium (a-$Si_{1-x}Ge_x$:H) alloys prepared by the plasma-enhanced, chemical-vapor-deposition technique with and without hydrogen dilution of the source gases (silane and germane) have been analyzed by small-angle x-ray scattering (SAXS), infrared vibrational spectroscopy, and flotation density measurements. Optoelectronic properties of codeposited films have also been characterized. Hydrogen dilution suppresses dihydride/polyhydride formation, reduces bonded H content, and reduces the SAXS-detected microstructure for $x>0$. Studies of anisotropy in the SAXS intensity indicate an increased amount of oriented microstructure as Ge is added, consistent with a trend toward columnarlike growth in both undiluted and hydrogen-diluted films, but the diluted films have a significantly reduced degree of such oriented microstructure. The improvement in the microstructure of a-$Si_{1-x}Ge_x$:H films by H_2 dilution correlates with concomitant improvement of optoelectronic properties. The modification of microstructure due to H_2 dilution of the source gases is discussed in terms of growth mechanisms of alloy films. © *1995 American Institute of Physics.*

I. INTRODUCTION

Alloying of hydrogenated amorphous silicon (a-Si:H) with germanium is a convenient method of matching the energy band gap (1.7–1.0 eV) to values consistent with device requirements. In particular, low-band-gap a-$Si_{1-x}Ge_x$:H layers are used in tandem with a-Si:H layers in solar cells to collect both low- and high-energy photons. The main drawback of this alloy is that its optoelectronic quality degrades with the decrease in band gap. Such degradation cannot be explained by increases in the midgap defect (dangling bond) density alone.[1–3] Several concepts have been introduced including two-phase heterostructure,[4] potential fluctuations,[5] and microstructure[6–9] to help understand the excess recombination of photogenerated carriers, other than via deep defect states. Improvement of steady-state photoconductivity of a fluorinated a-SiGe:H alloy, having almost the same deep defect density as the nonfluorinated alloy, has been explained with a two-phase heterostructure involving two transport paths.[10]

Mahan, Raboisson, and Tsu[11] suggested that in the case of C or Ge alloying of a-Si:H there is a recombination channel other than through midgap defects and they correlated this excess recombination with the presence of microstructure (local disorder) as detected by infrared (IR) vibrational spectroscopy. In the case of a-Si:H a quantitative measure of the amount of microstructure was introduced[6] as the parameter $R=I_{2080}/(I_{2000}+I_{2080})$, where I_{2080} and I_{2000} represent the IR absorbance at 2080 and 2000 cm^{-1}. Beyer,[12] through H diffusion and evolution experiments, established a correlation between the decay of optoelectronic properties of alloy films and the existence of weakly bonded or clustered H and interconnected microvoids. The latter were not detected directly, but inferred. The Hitachi group[13] has used small-angle x-ray scattering (SAXS) to indicate that a-SiGe:H alloys have a different microstructure than either a-Si:H or a-Ge:H based on a fractal analysis of the data. Jones *et al.*[7–9] have also noted increased SAXS for a-$Si_{1-x}Ge_x$:H alloys with $x>0.2$ but have interpreted the data in terms of increased amounts of microvoids or low-density, H-rich regions. However, the effect of hydrogen dilution on the SAXS-detected microstructure in such alloys has yet to be thoroughly studied and is therefore a major aspect of the present investigation.

Highly photoconductive a-$Si_{1-x}Ge_x$:H alloys with optical band gaps near and above 1.50 eV have been developed using a combination of low flow rates of the source gases and strong H_2 dilution as reported recently.[14] Detailed characterization of midgap defect and band-tail states reveals that the Urbach energy changes marginally while the deep defect density increases significantly with Ge incorporation.[15] Study of photogeneration and recombination in these alloys in a Pd/a-SiGe:H Schottky barrier structure reveals that the total recombination loss cannot be explained only by increases in neutral deep defect states [detected by electron spin resonance (ESR)].[16] On the other hand, similar values for the numbers of midgap states of the same sample measured by different techniques, such as photothermal deflection spectroscopy (PDS), the constant photocurrent method (CPM), ESR, and dual-beam photoconductivity (DBP), rule out the existence of a large density of charged defect states (D^+/D^-).[14–16] The recent evidence[8] of a direct role of microstructural defects (detected by SAXS) in degrading the

[a]Present address: Energy Conversion Devices, Inc., 1675 West Maple Road, Troy, MI 48084.
[b]Electronic mail: dwilliam@mines.edu

 0021-8979/95/78(8)/4966/9/$6.00

optoelectronic properties of a-$Si_{1-x}Ge_x$:H alloys for x up to about 0.4 merits further work. In this study we combine the techniques of SAXS, IR-absorption spectroscopy, and flotation density measurements to probe the microstructure of alloy films having optical band gaps from 1.7 to 1.2 eV ($x=0$ to $x=0.7$) prepared by plasma-enhanced chemical-vapor deposition (PECVD), with and without hydrogen dilution of the source gases.

II. EXPERIMENTAL DETAILS

A. Sample preparation

Series of a-$Si_{1-x}Ge_x$:H films have been prepared in a capacitively coupled, parallel-plate, 13.56 MHz radio-frequency (rf)-powered glow-discharge system with a diode configuration. Prior to deposition the reactor was baked to achieve a base pressure 10^{-7} Torr. Semiconductor-grade silane and germane (Matheson, 99.9999% purity) were used as source gases for the Si–Ge alloy films. The electrode on which the substrates were mounted was kept isolated from ground during deposition. Substrates included high-purity (99.999%) Al foil for the SAXS, crystalline Si wafers for the IR, and Corning 7059 glass for the optoelectronic measurements. Such samples were codeposited in a given run. The substrate temperature and rf power density were kept at 250 °C and 30 mW/cm^2, respectively. Two series of samples were prepared with increasing x. One series was made without H_2 dilution and the second was made with high (94%) H_2 dilution. For both series, the total flow rate of silane and germane were kept at the low value of 2.5 sccm and the value of x was varied by changing the gas flow ratio $[GeH_4/(GeH_4+SiH_4)]$. The chamber pressure was 0.2 Torr during preparation of the undiluted series and was 0.5 Torr for the H_2-diluted series.

B. Measuring techniques

The IR spectra were obtained with a Perkin Elmer 1750 Fourier transform IR (FTIR) spectrometer. Bonded H contents were calculated from the integrated absorption bands at 630 cm^{-1} (Si–H wag mode) and at 570 cm^{-1} (Ge–H wag mode) based on the calibration factors given in the review by Cardona.[17] The IR spectra were also deconvoluted to obtain values of the alloy microstructure parameter proposed by Mahan and co-workers,[11] for a-$Si_{1-x}Y_x$:H alloys,

$$R^*=[I_{2080}/(I_{2080}+I_{2000})](1-x) + [I_{Y\text{-}H_n}/(I_{Y\text{-}H_n}+I_{Y\text{-}H})]x,$$

where Y=Ge or C and $I_{Y\text{-}H_n}$ and $I_{Y\text{-}H}$ are the IR-absorption intensity analogs to the Si–H_n (at 2080 cm^{-1}) and Si–H (at 2000 cm^{-1}) stretching modes, respectively. It is difficult to isolate the absorption due to the Ge–H_2 stretch mode (~1975 cm^{-1}) from the Si–H stretch mode (2000 cm^{-1}) so a constant value of $I_{Ge\text{-}H_2}/(I_{Ge\text{-}H_2}+I_{Ge\text{-}H})=0.23$ was assumed for the Ge–hydrogen contribution.[11] The integrated intensity of the scissors/bending band at 750–950 cm^{-1} was also calculated to monitor the presence of dihydride and polyhydride bonds (Si–H_n and Ge–H_n, $n\geq 2$).

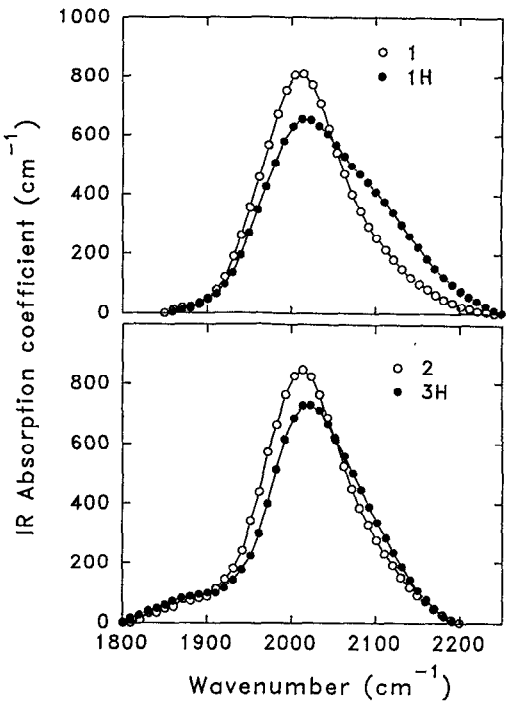

FIG. 1. Infrared vibrational spectra of the stretching mode for a-Si:H samples 1 and 1H and a-SiGe:H samples 2 and 3H.

The SAXS and flotation density measurements were made using procedures described in detail elsewhere.[7,18] To examine for anisotropic scattering, SAXS data were also collected with each sample tilted at 45° to the x-ray beam. Electron microprobe measurements on a small piece of each of the SAXS samples provided the value of x in each of the a-$Si_{1-x}Ge_x$:H alloys examined.

The steady-state secondary photoconductivity was measured under 50 mW/cm^2 white light from a tungsten lamp. Before each measurement the sample was annealed at 180 °C under vacuum (10^{-6} Torr) for 1 h. Transmittance and reflectance spectra were taken with a Hitachi 330 UV-VIS spectrophotometer and the optical gap was determined with the Tauc method.[19] The Urbach energy was determined by CPM.[20] The quantum efficiency–mobility–lifetime product $\eta\mu\tau$ was extracted from the photoconductivity measured under band-gap light using a wavelength where the absorption coefficient α was 10^{-3} cm^{-1} with a flux of 10^{15} cm^{-2} s^{-1}.

III. RESULTS

The IR-absorption bands corresponding to the stretch modes of the a-Si:H samples and two a-$Si_{1-x}Ge_x$:H alloys with optical gaps E_{opt} near 1.60 eV prepared with and without H_2 dilution are shown in Fig. 1. Under the H_2 dilution condition for $x=0$, there is a clear increase in the absorption near 2080 cm^{-1}, typically associated with either Si–H_2 configurations or Si–H on the internal surfaces of voids.[12,21] The bonded H content of the $x=0$ films increases from about 8.2 at. % to 9.3 at. % upon the use of H_2 dilution. The diluted sample with $E_{opt}=1.60$ eV ($x=0.22$) has slightly more of the 2080 cm^{-1} absorption than the undiluted sample and the ab-

TABLE I. Composition, band gap, IR, SAXS, and flotation density results for a-$Si_{1-x}Ge_x$:H alloys prepared with H_2 dilution (labeled no. H) and without dilution (labeled no). E_{opt} is the Tauc optical band gap. C_H is the bonded H content from the IR wag modes. R^* and I_{SB} are the microstructure factor and integrated intensity of the 750–900 cm^{-1} scissors/bend IR mode, respectively. Q_0 and Q_{45} are the integrated SAXS intensities obtained with the sample untilted and tilted at 45°, respectively. The film density and the density deficit relative to crystalline $Si_{1-x}Ge_x$ are d and $\Delta d/d_c$, respectively.

Sample	x	E_{opt} (eV)	C_H (at. %)	R^*	I_{SB} (a.u.)	Q_0 (10^{-6} nm^{-2})	Q_0/Q_{45}	d (g/cm^3)	$\Delta d/d_c$ (%)
1	0	1.71	8.2	0.14	0.036	0.71	1.3	2.25	3.4
1H	0	1.74	9.3	0.29	0.043	1.4	1.2	···	···
2	0.15	1.60	7.5	0.17	2.5	5.8	1.7	2.68	5.3
2H	0.22	1.60	7.5	0.18	3.4	1.5	1.5	2.89	5.6
3H	0.26	1.58	7.2	0.23	3.9	5.0	1.2	2.98	6.6
4H	0.34	1.52	6.4	0.19	···	3.1	3.1	3.26	5.2
3	0.37	1.44	7.2	0.25	8.3	7.3	2.6	3.32	6.2
5H	0.47	1.44	5.5	0.28	4.6	6.1	1.6	3.56	7.3
4	0.54	1.36	6.2	0.37	4.2	21	3.3	3.75	7.4
6H	0.57	1.35	4.3	0.37	2.3	14	2.3	3.94	4.8
7H	0.68	1.22	3.4	···	···	24	4.1	···	···
5	0.72	1.20	4.3	0.31	···	40	3.9	···	···

sorption band near 1875 cm^{-1} due to Ge—H bonds is noticeable. However, note that the amount of 2080 cm^{-1} absorption in the $x=0.22$ sample (3H) is noticeably reduced compared to the $x=0$ sample (1H). Although the two a-$Si_{1-x}Ge_x$:H films (2 and 3H) have similar band gaps (1.60 and 1.58 eV, respectively), the microprobe analysis shows the diluted film to have a significantly larger Ge content ($x=0.26$ vs 0.15). Similarly, for two films of smaller band gap, 1.44 eV, the Ge contents are again different, having values of $x=0.47$ and $x=0.37$ for the diluted and undiluted conditions. The Ge contents and optical gaps of all films studied are listed in Table I. The IR data from the two 1.44 eV films as well as those from lower-gap (~1.35 eV) material are shown in Fig. 2 for both the stretch modes and bending modes (750–900 cm^{-1}). Here one can see the clear increase in the Ge–H absorption due to the larger x of the diluted film and the reduced amount of dihydride/polyhydride bonding as a result of the dilution, despite the larger x for the two 1.44 eV films (3 and 5H). There is little evidence of a difference in the 2080 cm^{-1} absorption and deconvolution of the data shows R^* to be only slightly larger for the diluted film ($R^*=0.28$ vs 0.25).

In the case of the lower-band-gap film data of Fig. 2, the Ge contents are much closer, $x=0.57$ and 0.54 for the diluted and undiluted films (6H and 4), respectively. The Ge–H absorption is similar in intensity but there is slightly less of the 2080 cm^{-1} mode in the diluted film and there is a dramatic difference in the dihydride/polyhydride bonding to the Ge and Si as seen by the absorption band between 750 and 950 cm^{-1}. The bending mode IR data indicate nearly complete elimination of the Si–dihydride/polyhydride configurations using H_2 dilution, although much more Ge–H_n absorption shows up near 800 cm^{-1} to replace much of the Si–H_n absorption.

A summary of all the IR-determined results is provided in Table I. In general, the H_2 dilution induces clear changes in the H bonding configurations and affects the amount of Ge needed in the film to produce a given optical gap. The amount of dihydride/polyhydride bonding is significantly reduced in the lower-band-gap films (1.44–1.35 eV) as a result of the dilution. Note from the table that the bonded H content C_H was reduced slightly in every case except $x=0$ as a result of dilution. There is also a trend of less H incorporation with increased x. These trends will be considered in more detail later.

Figure 3 compares SAXS intensity data from three pairs of diluted and undiluted films with different x. The quantity $h=(4\pi/\lambda)\sin\theta$ is the magnitude of the x-ray scattering vector, where 2θ is the scattering angle relative to the incident beam and λ is the x-ray wavelength (0.154 nm). As dis-

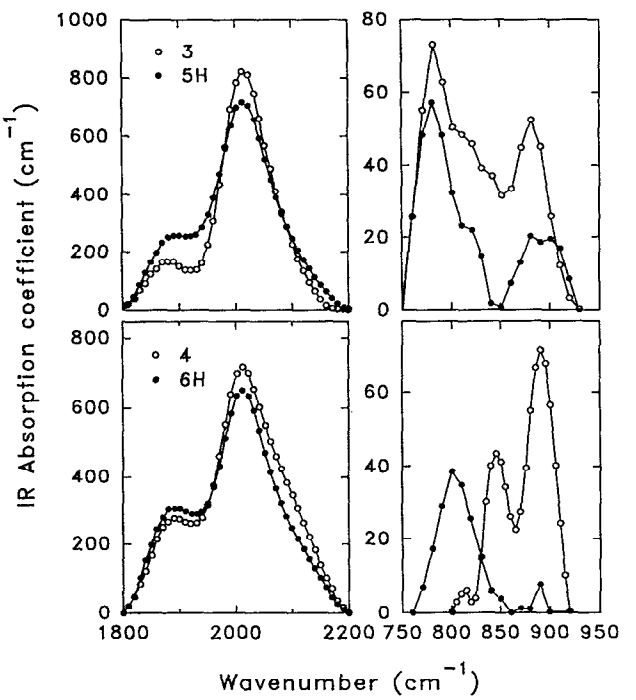

FIG. 2. Infrared vibrational spectra of the stretching (1800–2200 cm^{-1}) and scissors/bend (750–930 cm^{-1}) modes for a-SiGe:H samples 3 and 5H, and samples 4 and 6H.

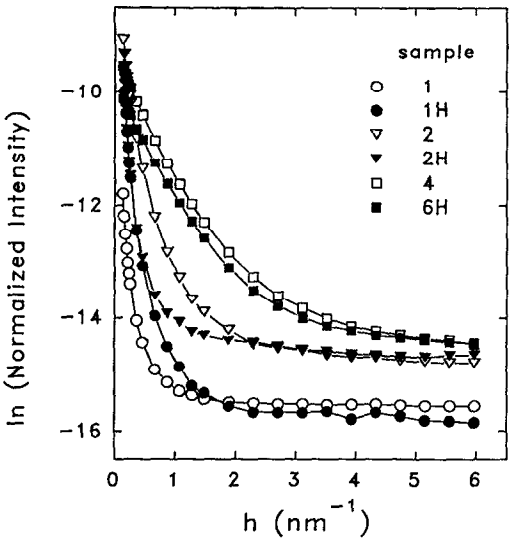

FIG. 3. SAXS intensities from three undiluted films compared with three H_2-diluted films.

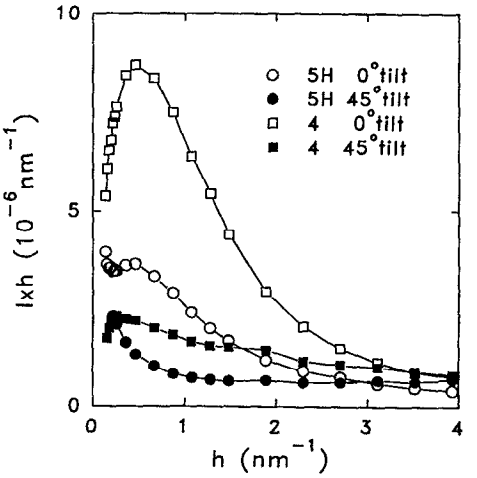

FIG. 5. SAXS tilting effect for one undiluted and one H_2-diluted film.

cussed previously,[8,9] there are two distinct contributions to the SAXS: the angle-dependent part due to electron-density fluctuations in the form of microvoids or low-density, H-rich material, and an angle-independent part due primarily to diffuse scattering from the alloy constituents on the atomic scale (so-called Laue monotonic scattering[22]). Both contributions can be seen to increase with increasing x in Fig. 3. The angle-independent contribution is carefully subtracted[23] to yield the angle-dependent scattering due to the microstructural inhomogeneities. The latter contribution is displayed Fig. 4 in the form of the product of the normalized SAXS intensity I and h versus h. This type of plot is useful since the area under this curve can be related quantitatively to the volume fraction of the scattering centers under simplifying assumptions:

(i) a two-phase system involving only two electron densities and therefore a single electron density difference Δn;

(ii) no preferred orientation of nonspherical scattering centers (and hence no anisotropic SAXS).

Then,

$$Q=\int Ih\,dh=\left(\frac{K}{\mu}\right)(\Delta n)^2 V_f(1-V_f), \tag{1}$$

where K is a constant determined by the geometry of the SAXS system and μ is the linear absorption coefficient of the sample. The latter quantity appears due to the method of intensity normalization used.[18]

Anisotropic scattering is observed in most of the samples so the above expression cannot be used directly to obtain a volume fraction, but Q remains useful as a measure of the amount of microstructure when coupled with another quantity: the ratio Q_0/Q_{45}, where Q_0 and Q_{45} are the integrated intensities obtained with the sample untilted (i.e., the film plane is perpendicular to the x-ray beam direction) and tilted at 45° relative to the x-ray beam, respectively. Model calculations have been performed for oriented, ellipsoidal-shaped scattering centers following procedures similar to those of Shibiyama *et al.*[24] in order to provide a first-order interpretation of the values of Q_0/Q_{45}. For example, ellipsoids with their long axis parallel to the film growth direction will produce $Q_0/Q_{45}>1$, consistent with experimental observations, and the values of Q_0/Q_{45} and Q_0 can provide estimates of the major-to-minor axis ratios of the ellipsoids, and the volume fraction of scattering centers. Under the assumption that the scattering centers are voids, then the void fraction obtained from the SAXS for such oriented, ellipsoidal voids can be compared with the density deficits obtained from the flotation density values of the same films.

Figure 5 shows the effect of tilting on the SAXS intensities for some of the films. In general the tilting effect (Q_0/Q_{45}) increases with x and it is less for the diluted films

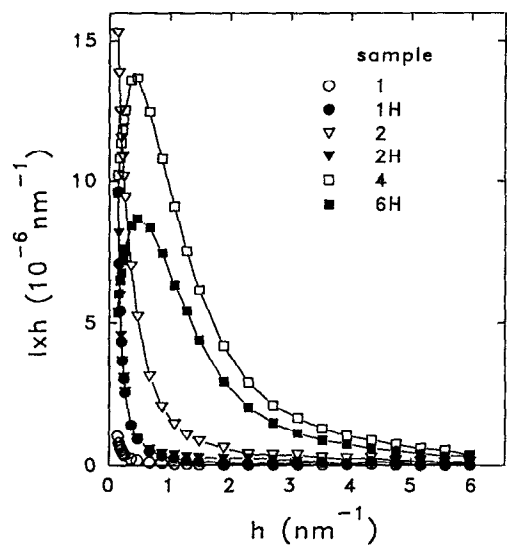

FIG. 4. SAXS $I\times h$ plots for same samples shown in Fig. 3. A constant background level was subtracted from each of the curves in Fig. 3 to obtain the intensities used here.

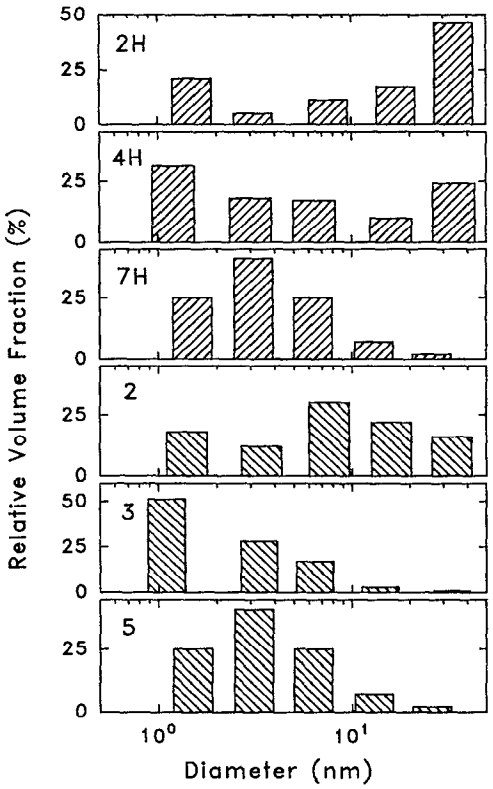

FIG. 6. Size distributions of scattering centers estimated from SAXS data obtained in the nontilted orientation.

with similar x. Table I includes the values of Q_0 and Q_0/Q_{45} for all of the alloys examined. Also shown are the flotation densities and the corresponding density deficits relative to crystalline $Si_{1-x}Ge_x$ alloys.[25] The flotation density could not be measured for the two highest Ge contents since the flotation fluid had a maximum density of 4.05 g/cm^3, corresponding to $x=0.60$ for crystalline alloys. The sample 1H could not be measured since the film broke into many small particles upon dissolving the Al–foil substrate, probably due to unusually high residual stress in this film.

The sizes of the scattering centers were estimated by fitting the SAXS data obtained with no tilting under the assumption of spherical shapes, using the spherical particle form factor,[26] and a distribution of radii. Due to the relatively small number of data points in each SAXS scan, the number of radii in the distributions was limited to five. Example results of such distributions are given in Fig. 6 where a clear increase in the fraction of scattering centers with diameters of 3–4 nm occurs with increasing x for both dilution conditions. The exact values of the individual diameters and fractions should not be taken too seriously in view of the simplified model used, but the trends should be valid. Since the tilt-dependent SAXS, which dominates the scattering from the high x alloys, is consistent with elongated scattering centers with their axes aligned with the film growth direction, this procedure will give the minor axis diameters of ellipsoids. An average major-to-minor axis ratio ν is estimated from the Q_0/Q_{45} values and these values together with the average minor axis diameters $\langle D\rangle$ and estimated volume fractions V_f are listed in Table II. Note that when the anisotropic scattering effect is modeled by the oriented ellipsoids the V_f are not very different for a given x.

The relatively large average sizes obtained from the two a-Si:H samples is due to the main SAXS signal seen in Fig. 3 as the steep rise at the smallest angles. There is little evidence of the 1-nm-size scattering centers sometimes detected in a-Si:H.[27,28] We do not think the steep SAXS signal at low h is due to microvoids with such large sizes but is likely due to either larger-scale H-concentration fluctuations or a surface roughness effect. The increased fraction of scattering centers with diameters of 3–4 nm with increasing x has been noted previously[7–9] for samples made by other groups. Thus, a-$Si_{1-x}Ge_x$:H alloys prepared by PECVD by several groups all show a similar type of microstructure and behavior versus x. The increased tilting effect versus x seen particularly for the undiluted films is also a general trend,[7–9] suggesting that oriented microstructure is unavoidable for $x>0.2$ (for all deposition conditions examined to date), although Q_0/Q_{45} is here significantly reduced by the H_2 dilution. As discussed earlier,[7–9] this oriented microstructure is associated with columnarlike growth, with the voids or low-density, H-rich regions between the columns being the origin the SAXS. The effect of the H_2 dilution seems to be the reduction in ν for a given x. Thus, the effect of dilution is apparently not to decrease strongly the volume fraction of the microvoids (Table II), but to decrease their aspect ratio, consistent with a reduced degree of columnarlike structure. This is examined more carefully below.

The optoelectronic properties obtained from the same codeposited films used for the SAXS measurements are listed in Table III. The Urbach width E_0, the photoconductivity σ_{ph}, and the quantum efficiency–mobility–lifetime

TABLE II. Size, shape, and void fraction results based on SAXS and model calculations assuming ellipsoidal-shaped scattering centers assuming the major axes are aligned perfectly with the growth direction. An average major-to-minor axis ratio ν was obtained from the Q_0/Q_{45} of Table I. The volume-fraction-averaged diameter $\langle D\rangle$ (in nm), represents the average minor axis diameter since this was determined from the SAXS scans at 0° tilt angle. V_f is the model-estimated void fraction (in vol %) based on the Q_0 and Q_0/Q_{45} in Table I.

Sample	1	2	3	4	5	1H	2H	3H	4H	5H	6H	7H
x	0	0.15	0.37	0.54	0.72	0	0.22	0.26	0.34	0.47	0.57	0.68
ν	1.6	2.4	4.2	5.5	6.7	1.4	2.0	1.4	2.0	2.2	3.6	7.0
$\langle D\rangle$	20	12	3.5	4.1	4.6	19	20	9	12	7	4.0	4.7
V_f	0.1	0.5	0.4	0.8	1.3	0.2	0.1	0.5	0.2	0.3	0.7	0.8

TABLE III. Optoelectronic properties. E_{opt} is the Tauc optical gap. E_0 is the Urbach energy. The conductivity measured in the dark and under illumination are indicated by σ_d and σ_{ph}, respectively. The quantity $\eta\mu\tau$ is the quantum efficiency–mobility–lifetime product.

Sample	E_{opt} (eV)	E_0 (meV)	σ_d ($10^{-9}/\Omega$ cm)	σ_{ph} ($10^{-4}/\Omega$ cm)	$\eta\mu\tau$ (10^{-5} cm^2/V)
1	1.71	46	2.9	5.6	2.0
1H	1.74	54	0.2	2.4	1.0
2	1.60	48	5.9	2.2	3.0
2H	1.60	50	4.0	2.1	1.6
3H	1.58	52	4.0	2.1	1.5
4H	1.52	51	12	0.51	0.6
3	1.44	55	11	0.57	0.07
5H	1.44	50	32	0.78	0.21
4	1.36	66	15	0.03	0.008
6H	1.35	60	51	0.19	0.07
7H	1.22	···	820	0.16	···
5	1.20	···	800	0.01	···

product $\eta\mu\tau$ are all regarded as useful monitors of the optoelectronic quality and one can see from the table a general degradation in these quantities with increasing Ge content.

IV. DISCUSSION

The focus of the present study is on the effects of H_2 dilution and we now consider several systematic trends in the data of Tables I, II, and III. A plot of the Q_0 vs x is useful for demonstrating a decreased amount of SAXS induced by the H_2 dilution as shown in Fig. 7(a). Its effect on Q_0/Q_{45} is considered in Fig. 7(b). There is a smooth, near-linear trend

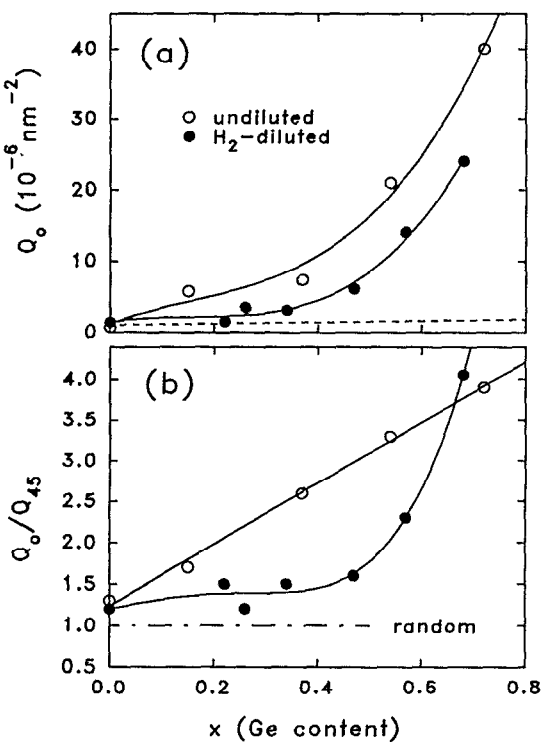

FIG. 7. (a) SAXS integrated intensities Q_0, vs Ge content, and (b) the tilting effect ratio Q_0/Q_{45} vs Ge content. Lines are drawn to guide the eye.

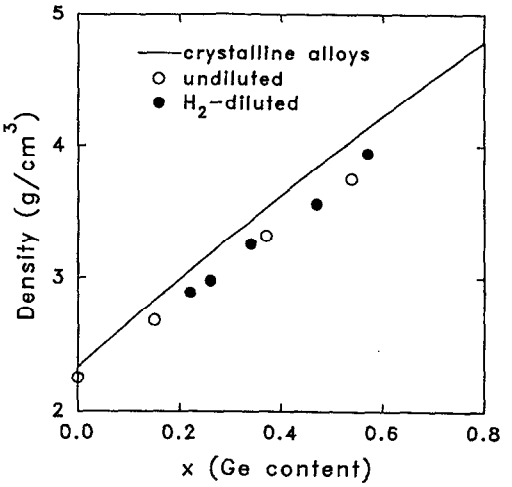

FIG. 8. Flotation densities of a-$Si_{1-x}Ge_x$:H alloys compared with crystalline $Si_{1-x}Ge_x$ (Ref. 25).

of Q_0/Q_{45} with x for the undiluted films and a clear reduction in this ratio for the diluted ones except at the highest Ge content. Q_0 is clearly reduced by the dilution for values of $x>0$. For the $x=0$ films, the amount of scattering is larger for the one produced with H_2 dilution. This result is opposite to those of previous measurements of a-Si:H films where decreased SAXS was observed with H_2 dilution.[29] It should be mentioned that due to a larger matrix electron density with increased Ge alloying, the value of Δn should increase with x, but this is compensated somewhat by the increase in μ [see Eq. (1)] such that the Q_0 should increase only slightly according to the dashed line in Fig. 7(a), assuming a fixed volume fraction of randomly oriented scattering centers similar to those in the $x=0$ films. Note that the changes observed are much larger than expected on this basis alone.

Figure 8 compares the measured film densities with those of crystalline $Si_{1-x}Ge_x$ alloys and there is no clear difference between the two type of films and this provides support for the model calculations of V_f shown in Table II where quite similar values are found for similar x. The density deficit has contributions from both the alloying of the amorphous network by the H and from the microvoids or low-density, H-rich regions. Only the latter produce the SAXS and the relatively small estimated void volume fractions (Table II) suggest a dominance of the H alloying effect on the deficits. There may also be an intrinsic density deficit due to an average difference in the bond length in the amorphous versus the crystalline state. It was recently demonstrated that a-Si (no H), produced by ion implantation, is $1.8\pm0.1\%$ less dense than crystalline Si,[30] suggesting an average bond length increase of 0.6% in the amorphous state.

The optical band gap and bonded H content C_H (as determined from the IR wag mode absorption) of the a-$Si_{1-x}Ge_x$:H films are plotted in Fig. 9 as a function of the Ge content x. For a-Si:H the C_H is larger for the diluted film, but there is a crossover near $x=0.2$ so that the undiluted films have more bonded H. A similar crossover does not occur in E_{opt}. The lower C_H for higher-x, diluted films versus the undiluted films may correlate with the reduced bend-

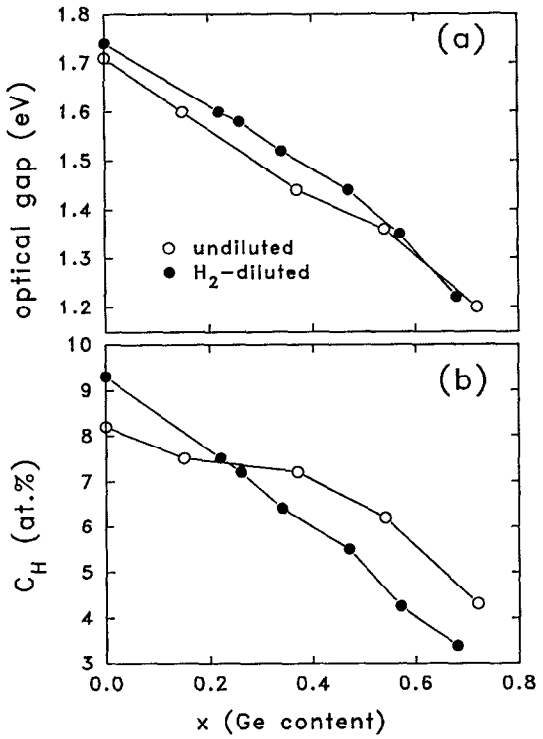

FIG. 9. Effect of H_2 dilution on (a) optical gap and (b) total bonded H content. Lines are drawn to guide the eye.

ing mode absorption corresponding to reduced fractions of the dihydride/polyhydride configurations (Fig. 2 and I_{SB} in Table I) and with the reduced amount of microstructure detected by SAXS (Fig. 7). There is no obvious difference in the IR-determined microstructure fraction R^* between the diluted and undiluted films above $x=0$. Note in Fig. 10 that the Urbach energy and the log of the photoconductivity suggest a transition to improved behavior with H_2 dilution for $x>0.2$, consistent with the dilution-induced improvement in SAXS-detected microstructure (Fig. 7). Comparison with C_H in Fig. 9 makes it clear that more bonded H (for a given x) correlates with poorer optoelectronic properties. This "extra" H is probably associated with the increased microvoids or H-rich regions detected by SAXS in the undiluted versus the diluted films.

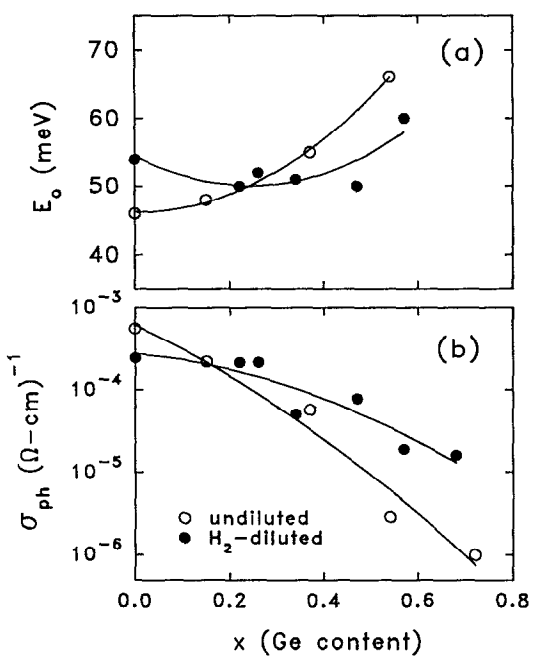

FIG. 10. Effect of H_2 dilution on (a) Urbach widths and (b) photoconductivities. Lines are drawn to guide the eye.

The exact correlation between SAXS and IR results is not well established for a-Si:H, although there does appear to be some connection between the $[SiH]_n$-induced appearance of the 2080 cm^{-1} stretch mode absorption and/or the 845–890 cm^{-1} scissors/bending mode absorption and enhanced SAXS-detected microstructure.[27] This issue is complicated by evidence that the 2080 cm^{-1} mode may also be due to Si—H bonds on the internal surfaces of voids,[21] which remains controversial.[31] Beyer[12] has shown by H evolution experiments that upon alloying with Ge or C, the low-temperature evolution peak increases while the high-temperature peak decreases. He attributed the decay of optoelectronic properties with alloying to the presence of an interconnected microvoid structure allowing desorption and diffusion of H_2 and hence to the low-temperature evolution peak. An anticorrelation was found between amount of voids (as inferred from the intensity of the low-temperature evolution peak) and the total hydrogen density (total evolved hydrogen) with Ge alloying, i.e., as the total hydrogen content decreased with x, the fraction evolving from voids increased. A similar behavior is found here in that C_H decreases with x [Fig. 9(b)] while the SAXS from voids or low-density regions increases for both undiluted and diluted films (Fig. 7), although less rapidly with x for the latter. There are reports regarding the role of H in modifying the network structure apart from reducing the defect density.[32,33] The multifaceted role of hydrogen remains unclear. Contrary to earlier belief, it has recently been shown that with reductions of the H content well below conventional levels, the tetrahedral amorphous network improves and this leads to improvement of optoelectronic properties and stability under prolonged illumination.[34,35]

It is observed in this study that in the case of a-Si:H ($x=0$), H_2 dilution of the source gases increases the dihydride/polyhydride bond formation, as seen by a doubling of the IR-determined value of R^*. The integrated SAXS intensity (Q_0, Table I) is also larger for this case. Thus, for the growth conditions used here, the microstructure of the $x=0$ film is not improved by the dilution, in contrast with a previous result.[29] This may be related to differences in deposition parameters.[36] Note also that the Urbach energy and the photoconductivity are degraded relative to the undiluted film (Fig. 10). A compact network structure with low H content in the undiluted $x=0$ and $x<0.2$ films can be understood from their growth kinetics. Since these films were grown with low flow rates of the source gases, the long residence time ensures creation of adequate amounts of atomic hydrogen within the chamber which takes an active role in network

reconstruction during growth by elimination of weak bonds and unwanted hydrogen. This leads to a more compact microstructure with less hydrogen. With an increased supply of atomic hydrogen brought about by the H_2 dilution the microstructure degrades.

However, the reverse trend is observed for the lower-band-gap alloys with $x>0.2$ such that the H_2 dilution becomes efficient in reducing the dihydride/polyhydride bonds and the microvoid densities. Thus the microstructure of low-band-gap a-$Si_{1-x}Ge_x$:H alloys improves significantly as a result of the hydrogen dilution method. A possible explanation of this behavior is as follows. The growing surface has a high fraction of Ge—H bonds and because of the weaker Ge—H bond strength compared to that of Si–H exodiffusion of surface hydrogen from Ge—H bonds occurs at the 250 °C deposition temperature.[37] The GeH_3 and SiH_3 radicals in the plasma contribute to the film growth at the low rates used here due to their long lifetime. Other radicals (SiH_2, GeH_2, etc.) are mostly converted to higher silane (Si_2H_6) or germane (Ge_2H_6) radicals via secondary reactions.[38,39] During growth under no dilution, the surface diffusion length of the dominant precursor becomes too short to allow the precursors to find the most energetically favorable sites. This is due to the large number of open dangling bond sites (Ge-) and the larger mass of the GeH_3 radical. Etching of weak bonds and clustered hydrogen is also reduced due to lack of sufficient atomic hydrogen. The low surface mobility and surface desorption rate of the surface radicals therefore leads to columnarlike growth with elongated voids (or low-density, H-rich regions) between the columns as well as the concurrent formation of polyhydride configurations.

Observations from *in situ* ellipsometric experiments[40] as well as from computer simulations[41] indicate that low surface mobility and desorption rate of surface radicals lead to a low-density network microstructure with voids, clusters, and polyhydrides, corroborating the above explanation. With the excess of hydrogen (94% dilution here), exodiffusion of surface hydrogen is counterbalanced by a greater supply of impinging hydrogen, thereby enhancing the surface mobility of incoming radicals. Thus, the growth of an alloy film at a slow deposition rate under H_2 dilution allows structural relaxation of the network. Consequently, hydrogen is incorporated predominately as monohydrides (Si-H). Moreover, under the presence of enhanced amounts of atomic hydrogen during growth, elimination of weak bonds and unwanted hydrogen occurs. In this process atomic hydrogen makes the overconstrained tetrahedral network of Si and Ge more flexible to satisfy most of the bonding requirements, resulting in a more relaxed, compact network structure. This leads to improved homogeneity in the form of reduced microvoid volume fractions and reduced polyhydride configurations. This in turn reduces the potential fluctuations and enhances the carrier drift mobilities. Such changes are seen through the increased steepness of the valence-band-tail states (indicated by the smaller E_0, Fig. 10) and improved photoconductivities and $\eta\mu\tau$ of the diluted films relative to the undiluted films with the higher Ge contents (Table III and Fig. 10).

Although we have chosen to display the trends of properties versus the Ge content, another approach is to examine the properties versus the optical gap since this is a crucial parameter in solar-cell behavior. One may compare the pairs of samples (2,2H), (3,5H), (4,6H), and (5,7H) in Tables I and III to see that above-discussed trends remain valid in that the diluted films of equal band gap are superior in optoelectronic quality and microstructure.

Finally, we recognize several other studies of the effects of H_2 dilution on the properties of a-$Si_{1-x}Ge_x$:H alloys.[42–54] For example, Matsuda *et al.*[44] observed that the photoconductivity under AM1 (100 mW/cm^2) was improved throughout the alloy region in the case of films prepared with a diode reactor. For a triode system, dilution was effective only for films with optical gaps $\geq$1.55 eV. Weller *et al.*[45] also deposited alloy films with diode and triode reactors, with and without H_2 dilution and found that use of the triode reactor with H_2 dilution led to AM1 photoconductivities of 2×10^{-4}–1×10^{-5} $(\Omega\,\mathrm{cm})^{-1}$ for optical gaps from 1.7 to 1.4 eV, respectively. Zeman *et al.*[53] observed strong effects of dilution for alloy films deposited in a diode reactor from mixtures of $GeH_4/(GeH_4+SiH_4)=0.2$ (corresponding to $x\simeq0.5$), where the ratio of light to dark conductivity increased by more than an order of magnitude as the dilution was increased from 50% to 95%. The increased dilution also reduced the Urbach energy. It was their speculation that this improvement was mainly due to the reduction of microstructure in the films associated with Si—H_2 bonding configurations such that a more structurally dense, void-free network is produced. The latter is confirmed by the present investigation, although significant amounts of microvoids remain at the highest Ge contents, even with dilution.

V. CONCLUSIONS

The microstructure of two series of a-$Si_{1-x}Ge_x$:H alloys prepared with and without hydrogen dilution has been characterized by small-angle x-ray scattering, infrared-absorption spectroscopy, and flotation density. The following conclusions are drawn from this study:

(1) Hydrogen dilution of source gases (silane and germane) modifies the microstructure in that less dihydride/polyhydride configurations and a weaker degree of columnarlike microstructure exist for the alloys with band gaps below about 1.6 eV. For the deposition conditions used here, hydrogen dilution induced slightly more microstructural features in the $x=0$ (a-Si:H) material, but at a relatively large size scale (~20 nm), not likely related to voids.

(2) Based on the SAXS made at 45° tilting, the microstructure changes from one of relatively good homogeneity at low x to one of columnarlike structure with elongated voids (or low-density, H-rich regions) oriented with their long axes parallel to the growth direction at high x.

(3) As Ge is added, the size distribution of the scattering centers changes to one that can be modeled with ellipsoidal voids with minor-axis diameters that are predominantly 3–4 nm and and major-to-minor axis ratios as high as 7 for the largest Ge contents. The modeling suggests that hydrogen dilution tends to reduce the aspect ratio of the ellipsoids rather than decreasing the void volume fraction.

(4) The loss of bonded H induced by hydrogen dilution is accompanied by higher Ge content to yield the same optical band gap for the range from about 1.6 to 1.4 eV, an unexpected behavior since both reduced H and increased Ge typically reduce the band gap.

(5) The improved microstructure seen with hydrogen dilution at the larger Ge contents or smaller optical band gaps correlates with improved optoelectronic behavior.

ACKNOWLEDGMENTS

The work at IACS was carried out under a project funded by the United Nations Development Programme and the Ministry of Non-Conventional Energy Sources, Government of India. The work at Colorado School of Mines was supported by the National Renewable Energy Laboratory under Contract Nos. XG-1-10063-3 and XAN-4-13318-04. The help of Yan Chen with the SAXS measurements and analyses is appreciated. Electron microprobe measurements of the Ge contents by A. Mason of NREL are gratefully acknowledged.

[1] K. D. MacKenzie, J. R. Eggert, D. J. Leopold, Y. M. Li, S. Lin, and W. Paul, Phys. Rev. B **31**, 2198 (1985).
[2] S. Ajishi, Z. E. Smith, and S. Wagner, in *Amorphous Silicon and Related Materials*, edited by H. Fritzsche (World Scientific, Singapore, 1986), p. 887.
[3] H. G. Bauer, C. E. Nebel, M. B. Schubert, and G. Schumm, Mater. Res. Soc. Symp. Proc. **149**, 485 (1989).
[4] K. D. MacKenzie and W. Paul, J. Non-Cryst. Solids **97&98**, 1055 (1987).
[5] B. von Roedern and A. Madan, Philos. Mag. B **63**, 293 (1991).
[6] D. Jousse, E. Bustarret, and F. Boulitrop, Solid State Commun. **55**, 435 (1985).
[7] S. J. Jones, Y. Chen, D. L. Williamson, and G. D. Mooney, Mater. Res. Soc. Symp. Proc. **258**, 229 (1992).
[8] S. J. Jones, Y. Chen, D. L. Williamson, R. Zedlitz, and G. Bauer, Appl. Phys. Lett. **62**, 3267 (1993).
[9] S. J. Jones, Y. Chen, D. L. Williamson, X. Xu, J. Yang, and S. Guha, Mater. Res. Soc. Symp. Proc. **297**, 815 (1993).
[10] K. D. MacKenzie, J. H. Burnett, J. R. Eggert, Y. M. Li, and W. Paul, Phys. Rev. B **38**, 6120 (1988).
[11] A. H. Mahan, P. Raboisson, and R. Tsu, Appl. Phys. Lett. **50**, 335 (1987).
[12] W. Beyer, J. Non-Cryst. Solids **97&98**, 1027 (1987).
[13] S. Muramatsu, T. Shimada, H. Kajiyama, K. Azuma, T. Watanabe, T. Kamiyama, and K. Suzuki, Jpn. J. Appl. Phys. **28**, L1092 (1989).
[14] A. R. Middya, S. C. De, and S. Ray, J. Appl. Phys. **73**, 4622 (1993).
[15] J. K. Rath, A. R. Middya, and S. Ray, Philos. Mag. B **71**, 851 (1995).
[16] P. Chaudhuri, A. R. Middya, and S. Ray, Sol. Cells and Sol. Energy Mater. **30**, 233 (1993).
[17] M. Cardona, Phys. Status Solidi B **118**, 463 (1983).
[18] D. L. Williamson, A. H. Mahan, B. P. Nelson, and R. S. Crandall, Appl. Phys. Lett. **55**, 783 (1989).
[19] J. Tauc, in *Amorphous and Liquid Semiconductors*, edited by J. Tauc (Plenum, New York, 1974), p. 159.
[20] M. Vanecek, J. Kocka, J. Stuchlik, Z. Kozisek, O. Stika, and A. Triska, Sol. Energy Mater. **8**, 411 (1983).
[21] H. Wagner and W. Beyer, Solid State Commun. **48**, 585 (1983).
[22] See, for example, L. H. Schwartz and J. B. Cohen, *Diffraction from Materials* (Springer, Heidelberg, 1987), p. 402.
[23] K. Müller, in *Small Angle X-ray Scattering*, edited by O. Glatter and O. Kratky (Academic, New York, 1982), p. 232.
[24] M. Shibiyama, S. Nomura, T. Hashimoto, and E. L. Thomas, J. Appl. Phys. **66**, 4188 (1989).
[25] J. P. Dismukes, L. Ekstrom, and R. J. Paff, J. Phys. Chem. **68**, 3021 (1964).
[26] A. Guinier and G. Fournet, *Small-Angle Scattering of X-rays* (Wiley, New York, 1955).
[27] S. Chattopadhyay, S. N. Sharma, R. Banerjee, D. M. Bhusari, S. T. Kshirsagar, Y. Chen, and D. L. Williamson, J. Appl. Phys. **76**, 5208 (1994).
[28] S. Guha, J. Yang, S. J. Jones, Y. Chen, and D. L. Williamson, Appl. Phys. Lett. **61**, 1444 (1992).
[29] A. J. M. Bernsten, M. J. Van den Boogaard, W. G. J. H. M. Van Sark, and W. F. Van der Weg, Mater. Res. Soc. Symp. Proc. **258**, 275 (1992).
[30] J. S. Custer, M. O. Thompson, D. C. Jacobson, J. M. Poate, S. Roorda, W. C. Sinke, and F. Spaepen, Appl. Phys. Lett. **64**, 437 (1994).
[31] J. Daey Ouwens, R. E. I. Schropp, and W. F. Van der Weg, Appl. Phys. Lett. **65**, 204 (1994).
[32] W. B. Jackson, Phys. Rev. B **41**, 1059 (1990).
[33] D. Das, H. Shirai, J. Hanna, and I. Shimizu, Jpn. J. Appl. Phys. **30**, L239 (1991).
[34] H. Shirai, K. Nakamura, J. Hanna, and I. Shimizu, J. Non-Cryst. Solids **137&138**, 653 (1991).
[35] A. H. Mahan and M. Vanecek, in *Amorphous Silicon Materials and Solar Cells*, edited by B. L. Stafford, AIP Conf. Proc. No. 234 (AIP, New York, 1991), p. 195.
[36] J. Daey Ouwens, R. E. I. Schropp, C. H. M. Van der Werf, M. B. Von der Linden, C. H. M. Maree, W. F. Van der Weg, P. Rava, F. Demichelis, C. F. Pirri, and E. Tresso, Mater. Res. Soc. Symp. Proc. **297**, 61 (1993).
[37] K. Tanaka and A. Matsuda, Thin Solid Films **163**, 123 (1988).
[38] A. Matsuda and K. Tanaka, J. Appl. Phys. **60**, 2351 (1986).
[39] A. R. Middya and Swati Ray, J. Appl. Phys. **75**, 734 (1994).
[40] R. W. Collins and J. M. Cavese, J. Appl. Phys. **61**, 1869 (1987).
[41] M. J. McCaughey and M. J. Kushner, J. Appl. Phys. **65**, 186 (1989).
[42] S. Guha, K. L. Narasimhan, and S. M. Pietruszko, J. Appl. Phys. **52**, 859 (1981).
[43] D. Slobodin, S. Aljishi, Y. Okada, D.-S. Shen, V. Chu, and S. Wagner, Mater. Res. Soc. Symp. Proc. **70**, 275 (1986).
[44] A. Matsuda, K. Yoggi, M. Koyama, M. Toyama, Y. Imanishi, N. Ikuchi, and K. Tanaka, Jpn. J. Appl. Phys. **25**, L54 (1986).
[45] H. C. Weller, S. M. Paasche, C. E. Nebel, and G. H. Bauer, J. Non-Cryst. Solids **97&98**, 1071 (1987).
[46] T. Ishihara, S. Terazono, H. Sasaki, K. Kawabata, T. Itagaki, H. Morikawa, M. Deguchi, K. Sato, M. Usui, K. Okaniwa, M. Aiga, M. Otsubo, and K. Fujikawa, in *Proceedings of the 19th IEEE Photovoltaic Specialists Conference* (IEEE, New York, 1987), p. 749.
[47] K. Tanaka and A. Matsuda, Mater. Sci. Rep. **2**, 139 (1987).
[48] L. Mariucci, F. Ferrazza, D. Della Sala, M. Capizzi, and F. Evangilisti, J. Non-Cryst. Solids **97&98**, 1075 (1987).
[49] J. Wind, G. Krötz, V. Petrova-Koch, G. Müller, and P. P. Deimel, J. Non-Cryst. Solids **114**, 531 (1989).
[50] A. Catalano, in *Proceedings of the 21st IEEE Photovoltaic Specialists Conference* (IEEE, New York, 1990), p. 36; M. S. Bennett, A. Catalano, K. Rajan and R. R. Arya, *ibid.*, p. 1653.
[51] C. Godet, V. Chu, B. Equer, Y. Bouizem, L. Chahed, I. El Zawawi, M. L. Theye, S. Basrour, J. C. Bruyere, and J. P. Stoquert, Mater. Res. Soc. Symp. Proc. **192**, 163 (1990).
[52] Y. S. Tsuo, Y. Xu, E. A. Ramsay, R. S. Crandall, S. J. Salamon, I. Balberg, B. P. Nelson, Y. Xiao, and Y. Chen, Mater. Res. Soc. Symp. Proc. **219**, 769 (1991).
[53] M. Zeman, I. Ferreira, M. J. Geerts, and J. W. Metselaar, Sol. Energy Mater. **21**, 255 (1991).
[54] F. Zang, Z. Song, Y. Guo, and G. Chen, Sol. Cells Sol. Energy Mater. **29**, 195 (1993).